



CHORUS

This is the accepted manuscript made available via CHORUS. The article has been published as:

Noninductively Driven Tokamak Plasmas at Near-Unity Toroidal Beta

D. J. Schlossberg, G. M. Bodner, M. W. Bongard, M. G. Burke, R. J. Fonck, J. M. Perry, and J. A. Reusch

Phys. Rev. Lett. **119**, 035001 — Published 18 July 2017

DOI: [10.1103/PhysRevLett.119.035001](https://doi.org/10.1103/PhysRevLett.119.035001)

Non-Inductively Driven Tokamak Plasmas at Near-Unity Toroidal Beta

D.J. Schlossberg,* G.M. Bodner, M.W. Bongard, M.G. Burke, R.J. Fonck,
J.M. Perry, and J.A. Reusch

Department of Engineering Physics, University of Wisconsin-Madison,

1500 Engineering Drive, Madison, WI 53706, USA

Access to and characterization of sustained, toroidally confined plasmas with very high plasma-to-magnetic pressure ratio (β_t), low internal inductance, high elongation and non-solenoidal current drive is a central goal of present tokamak plasma research. Stable access to this desirable parameter space is demonstrated in plasmas with ultra-low aspect ratio and high elongation. Local helicity injection provides non-solenoidal sustainment, low internal inductance, and ion heating. Equilibrium analyses indicate β_t up to $\sim 100\%$ with a minimum $|B|$ well spanning up to $\sim 50\%$ of the plasma volume.

Magnetic confinement fusion relies on balancing outward pressure from thermonuclear plasma with inward, confining pressure from applied magnetic fields. In a tokamak, the leading fusion reactor candidate, a useful metric for confinement efficacy is the ratio of kinetic to magnetic pressure, quantified by toroidal beta $\beta_t = \langle p \rangle / (B_{t0}^2 / 2\mu_0)$. Here $\langle p \rangle$ is the volume-averaged plasma pressure and B_{t0} is the applied vacuum toroidal magnetic field at the plasma geometric axis R_0 . Since fusion power scales with β_t^2 for a given toroidal magnetic field, operation at high β_t is a longstanding goal of the international fusion program [1, 2].

The spherical tokamak (ST) is a low-aspect ratio ($A \equiv R_0/a < 2$) variant of the toroidal tokamak geometry that offers the possibility of very high β_t operation in a compact size [3], and may provide a high fusion neutron flux source [4] or possibly an attractive fusion energy source [5]. The extreme toroidicity of the ST provides stable confinement at high normalized plasma current I_N .

The achievement of high stable β_t must be accompanied by operation with a high fraction of self-generated bootstrap current to realize fusion-relevant steady-state operation. This occurs at high normalized beta $\beta_N = \beta_t a B_{t0} / I_p \equiv \beta_t / I_N$, where a is the plasma minor radius, and I_p is the plasma current [MA] [1, 3]. Access to high β_N within MHD stability limits is available from low- A plasma configurations with high elongation κ and low internal inductance ℓ_i [6]. Operation at near-unity A provides ready access to high κ , but adds challenges of generating and sustaining the plasma without solenoidal induction [7]. Thus, a major scientific goal of STs worldwide is accessing and evaluating a state of high β_t and β_N , high κ , low ℓ_i , and low collisionality without use of solenoidal current drive [1].

This Letter demonstrates first access to this interesting fusion plasma state for several energy confinement times. It is accessed in a near-unity aspect ratio tokamak by employing a

novel local helicity injection (LHI) technique to initiate, sustain, and heat a toroidal plasma without solenoidal induction.

Operating at the very low B_t allowed at $A \sim 1$, with hollow current profiles afforded by the LHI process, provides access to extremely high $\beta_t \sim 100\%$. Additionally, it offers the possibility of creating an absolute minimum- B well over much of the plasma cross-section. Such wells may improve stability, fast ion confinement, and/or auxiliary heating efficiency.

These experiments were performed on the ultralow- A Pegasus Toroidal Experiment [8]. It is a mid-sized spherical tokamak with $I_p < 0.25$ MA, $B_{t0} < 0.19$ T, $I_{TF} < 0.288$ MA, $R_0 \sim 0.35$ m, $a \sim 0.30$ m, $\kappa = 1-3$, and $\Delta t_{pulse} \leq 25$ ms. Its $A \geq 1.16$ configuration provides MHD stability at $I_N > 5$ and low B_{t0} without wall stabilization [9]. At the T_e attained during operation at this low B_t in a relatively small experiment, the electron collisionality is usually higher than desired for fusion applications. Nevertheless, plasmas achieved here allow assessment of the general properties and macroscopic MHD stability of this interesting plasma regime. Access to high β_t is facilitated by operation at $B_{t0} \sim 0.03$ T and auxiliary plasma heating from LHI. The highest β_t plasmas are realized by further reducing B_t during the discharge, a technique employed in earlier, higher- A experiments in NSTX [10], START [11], and DIII-D [12, 13].

High- β_t plasmas studied here are initiated and driven by the LHI technique, in which strong localized electron currents injected along magnetic field lines in the plasma edge relax through helicity-conserving magnetic turbulence to form a tokamak-like plasma [14]. LHI can then continue to drive and sustain these plasmas, or they can be readily coupled to auxiliary current drive [15, 16]. The present experiments employed two injectors located near the bottom of the plasma at 0.26 m major radius. Contrary to earlier studies using outboard low-field side

injection [12], this results in plasma initiation and growth at approximately constant major radius. Changes in shape during the plasma growth induce a net negative current drive which offsets any residual positive drive from the rising equilibrium (vertical) vacuum field. Hence, these plasmas are non-inductively driven throughout the discharge.

LHI additionally facilitates access to high β_t by driving strong edge currents that produce a favorable safety factor (q) profile. It drives strong edge shear, $q_0 > 2$ in the core, and $\ell_i < 0.3$. These characteristics improve MHD stability. Recent work has shown LHI also fortuitously provides magnetic-reconnection-driven ion heating that increases the total plasma pressure without a separate ion heating source [17]. Impurity ion temperature measurements indicate T_{i0} is typically 1–3 times T_{e0} during LHI.

Figure 1 shows discharge parameters for high- β_t scenarios employing either constant- (red dashed) or ramped (black solid) $B_t(t)$. $I_p = 0.1$ MA was generated and sustained non-inductively via LHI using 7 kA of injected current (I_{inj}) [Fig. 1(a)]. Fueling throughout the discharge resulted in steadily increasing line-averaged density $\bar{n}_e \leq 1.3 \times 10^{19} \text{ m}^{-3}$ [Fig. 1(b)]. Central electron and ion temperatures [Fig. 1(c)] were measured using multi-point Thomson scattering [18] and passive impurity spectroscopy [19], respectively. Reconnection-driven ion heating from LHI yielded $T_{i,OV}(0) \sim 150\text{--}300$ eV, exceeding $T_e(0) \sim 100$ eV throughout the discharge. Large-scale MHD activity was evident on low-field-side Mirnov coils [Fig. 1(d)]. It is especially large at early times, following the initial relaxation to a tokamak-like configuration. A plasma disruption in ramped- B_t discharges is precipitated by a rapidly-growing MHD event [Fig 1(d), ~ 25 ms]. In contrast, constant- B_t plasmas are sustained until LHI drive is removed (26 ms for both cases).

Equilibrium reconstructions of these plasmas determine relevant properties such as β_t , β_N , and ℓ_i . All reconstructions employ external magnetic constraints. Earlier work showed β_t obtained via this method had a relative uncertainty $\leq 15\%$ [20]. Here, reconstructions of discharges with Thomson scattering and impurity spectroscopy measurements are further constrained by specifying the average total pressure in the plasma core ($0.354 \text{ m} < R_0 < 0.415 \text{ m}$) and the location of the plasma edge, defined by an inflection in $p_e(R)$. A sensitivity study was performed to examine possible open-field-line current effects by using I_p values reduced by I_{inj} times its toroidal windup factor. The measurements were best fit when the total I_p resided on closed flux surfaces, while reconstructions with reduced I_p had substantially higher χ^2 . Variations in β_t were $<10\%$ throughout the sensitivity study.

Figure 2(a) shows a kinetically-constrained reconstruction of an $A = 1.21$, highly elongated plasma ($\kappa = 2.6$) near the end of a ramped- B_t discharge that attained $\beta_t = 95\%$, $\beta_N = 6.7$, and $I_N = 14$. The safety factor profile, current density profile, and equilibrium parameters are given in Fig. 2(b)–(d), respectively. These plasmas feature a hollow current profile with very low internal inductance ($\ell_i = 0.22$) and remain paramagnetic, with a modest poloidal beta $\beta_p \equiv \langle p \rangle / \bar{B}_{p,a}^2 = 0.45$. Similarly kinetically-constrained reconstructions of the constant- B_t scenario indicate $\beta_t \leq 35\%$, $\beta_N \sim 3$, and $\ell_i \sim 0.3$. Simple application of the Sauter model [21] suggests bootstrap current fractions of at most 20%, distributed evenly across the plasma cross-section.

Figure 3 shows representative electron temperature, density, and pressure profiles near the end of ramped- B_t scenarios corresponding to the reconstruction in Fig. 2. The central impurity (OV) ion temperature is also indicated in Fig. 3(a). These profiles were obtained by scanning the Thomson scattering diagnostic's observation locations across the plasma radius in

repeated discharges. The \bar{n}_e calculated from these absolutely calibrated Thomson scattering measurements agreed with microwave interferometry within experimental uncertainty. These very high β_t plasmas were extremely reproducible; several hundred repeated discharges were taken with close agreement in I_p , T_e , shaping, MHD amplitudes, etc.

In general, the $T_e(R, t)$ profile is seen to flatten as the density rises in these discharges. Nevertheless, $p_e(R)$ is peaked due to density peaking. The peak in $p_e(R)$ often lies inside the reconstructed magnetic axis, R_m , while $T_i(R)$ is typically higher outside R_m . These ion temperature measurements, derived from tangential chordal sightlines, imply the estimated total (i.e., single-fluid) pressure peaks near R_m . Future studies addressing specifics of the kinetic profiles will require additional diagnosis, but will likely have little influence on total pressure estimates and global discharge characteristics.

Kinetically-constrained reconstructions of both discharge scenarios were performed at all times that internal measurements were available. To more fully represent the broader β_t - I_N space attained experimentally, magnetics-only reconstructions at these times were compared to the better-constrained kinetic cases. Magnetics-only cases systematically overestimated β_t by 10–30%. This likely arises from poorer constraint on the plasma size due to the large separation of the plasma edge from the outboard magnetic diagnostics. To account for this systematic overestimate, β_t values obtained at times without kinetic measurements were conservatively reduced by an average, constant scaling factor of 0.71. Trends in $\beta_t(t)$ were similar for equilibria obtained with partial kinetic and magnetics-only measurements.

Figure 4 shows the β_t - I_N space accessed in Pegasus in a Troyon stability plot. Solid markers denote values from reconstructions using partial-kinetic constraints while open symbols indicate reconstructions using scaled magnetic measurements only, as described above. The

operating space of several high- β_t tokamak experiments and lines of nominally-bounding β_N values are shown for reference. The operating space for high- A tokamaks (green hatched region) is bounded by $\beta_t \sim 10\%$, $I_N \sim 3$ [22]. Low- A tokamaks such as START [23] and NSTX [10] have accessed $\beta_t \sim 40\%$, $I_N \sim 8$ (blue solid region). We also note the TS-3 device has reported $40\% < \beta_t < 100\%$ for $I_N \leq 9$ in merging plasma experiments, but for transient discharge lengths much less than an inferred confinement time [24].

The present experiments sustain world-record β_t values by accessing extremely high I_N , which is enabled by operation at $A \sim 1.2$. For constant- B_t scenarios (circles in Fig. 4), $\beta_t \lesssim 55\%$ at $I_N \sim 10$ is achieved. In B_t rampdown scenarios (triangles) I_N and β_t increased accordingly, indicated by the progression of values upward from $I_N \sim 10$ to 14 and β_t from $\sim 40\%$ to 100%.

With continued decrease in B_t , plasmas eventually became unstable and disrupted. This disruptive event shows a rapidly increasing oscillation on Mirnov coil signals, followed by the plasma termination, depicted in Fig. 5(a). The rapid growth and $\sim 100 \mu\text{s}$ timescale of the terminating event suggests violation of an ideal MHD stability limit.

The mode structure of the disruptive event was inferred using cross-phase analysis of toroidal and poloidal Mirnov coil arrays. Toroidal spectral analysis indicates events have a toroidal mode number $n = 1$. To accommodate strong poloidal shaping and high- β_t effects, poloidal cross-phase analyses employed a PEST straight-field-line angular mapping [25] and q -values from equilibrium reconstructions. For the time just prior to the disruption, a least-squares search for best-fit m and flux surface location gives $m = 9 (+2/-3)$ and a resonant surface near the plasma boundary at $\sqrt{\psi_N} \sim 0.9$ (where the normalized flux surface label $\psi_N(R_0) = 0$ and $\psi_N(a) = 1$).

The ideal MHD stability of these discharges was analyzed using the DCON code [26]. Two sets of model equilibria were generated based on kinetically-constrained reconstructions for the constant- B_t and ramped- B_t cases. The no-wall, ideal MHD β_N limit for each case was identified by increasing $\langle p \rangle$ with fixed bulk plasma parameters (geometry, I_p , ℓ_i). Above a critical $\beta_{N,limit}$, discharges became unstable to $n = 1$ perturbations. The constant- B_t scenario is stable with $\beta_N = 3.2 \sim \beta_{N,limit}/2$. In contrast, the disruptive ramped- B_t scenario was at best marginally stable, with $\beta_N = 6.5 \sim \beta_{N,limit}$.

Analysis of the marginally unstable poloidal harmonic structure from DCON in the ramped- B_t scenario showed dominant components with $4 < m \lesssim 10$ near $\sqrt{\psi_N} \sim 0.9$ [Fig 5(b)]. The similarity between experimental and model mode numbers suggests the ramped- B_t discharges terminate at the ideal no-wall β limit. The unstable flux surface location and the finite- m numbers suggest the disruptive mode structure is that of an external kink instability.

Equilibrium reconstructions indicate these high- β_t discharges contain broad “magnetic wells,” or regions with a minimum in total $|B|$ [27, 28]. Figure 6(a) depicts isocontours of ψ_N (dotted blue) and $|B|$ (solid black) for the equilibrium of Fig. 2. A minimum $|B|$ region with closed contours is present over 47% of the confined plasma volume (shaded red). Figure 6(b) shows a radial profile of magnetic field components at the plasma midplane, where the minimum $|B|$ region is present between $0.31 \text{ m} < R < 0.58 \text{ m}$. The well broadens and deepens as $B_t(t)$ is reduced, while in static- B_t discharges the well shape remains nominally constant. Magnetic wells persist several times longer than expected energy confinement times, and are very robust features of these equilibrium reconstructions. This robustness derives from the combination of low B_t , very low ℓ_i , and moderate core pressure, all of which are readily constrained by available measurements.

Such absolute minimum-B regions have been considered theoretically. The reversal of ∇B driven drifts within the magnetic well can stabilize otherwise unstable drift modes [29, 30]. This suggests turbulence and transport may be reduced in such regions. In addition, stochastic transport of energetic ions has been shown to be reduced [31]. High-energy fusion alpha particles may be better-confined by these structures [32]. Finally, simulations of neutral beam injected energetic ions show that magnetic wells can greatly reduce prompt losses [33, 34].

The influence of operation at $A \sim 1$, hollow current profiles at very low ℓ_i and B_t , and moderate core pressure on access to absolute minimum-B is elucidated by examining components of \mathbf{B} in Fig. 6(b).

At high I_N , the increased elongation of low- A plasmas leads to a proportionally larger poloidal field contribution to $|B|$ than at higher A . This occurs because $I_N \propto \sqrt{(1 + \kappa^2)} B_p/B_t$, and is evident in Fig. 6(b). Outboard of the magnetic axis, the rapidly increasing B_p provides a large contribution to $|B|$. However, studies of model equilibria indicate high I_N alone does not generate a substantial magnetic well until extreme values are reached ($I_N > 25$). The hollow current profiles driven by LHI also strongly contribute to the well formation, since the resulting poloidal field increases rapidly from the core to the edge.

Though plasmas here remain paramagnetic ($\beta_p < 1$), increased diamagnetism as $\beta_p(t)$ rises serves to reduce B_t near the core. A pressure-driven increase in Shafranov shift also pushes the peak $|B_p|$ outboard toward regions of lower B_t , facilitating well formation and increasing its depth. These effects are analogous to those that may lead to magnetic wells at high- A due to plasma diamagnetism at very high β_p [35]. The main difference here is the relatively easy access to regions of large-volume absolute minimum-B afforded by operation at near-unity A using local helicity injection.

Demonstration of access to very high β_t at near-unity A opens new opportunities to test our understanding of magnetically confined plasmas. This Letter demonstrates the ability to access configurations with high elongation, $\beta_t \sim 100\%$, low ℓ_i , and non-inductive sustainment. Stability properties to date conform to predicted no-wall ideal MHD stability limits. Finally, access to a unique operating space with large magnetic wells, which may offer enhanced energetic particle confinement and/or reduced turbulence, has been demonstrated. This offers possibilities for future studies of this interesting high β_t regime.

The enthusiastic support and insight of T.S. Taylor is gratefully acknowledged. The authors thank B.A. Kujak-Ford, G.R. Winz, N.J. Richner, and C. Rodriguez Sanchez for their technical assistance, and wish to acknowledge useful conversations with C.C. Hegna, J.D. Callen, and J.L. Barr. This material is supported by the U.S. Department of Energy, Office of Science, Office of Fusion Energy Sciences, under Award No. DE-FG02-96ER54375. Any opinions, findings, and conclusions or recommendations expressed in this publication are those of the authors and do not necessarily reflect the views of the U.S. Department of Energy. Data from this publication are publicly available in openly documented, machine-readable formats [36].

-
- [1] M. Ono and R. Kaita, *Phys. Plasmas* **22**, 040501 (2015).
 - [2] T.C. Hender *et al.*, *Nucl. Fusion* **47**, S128 (2007).
 - [3] Y.-K.M. Peng, and D.J. Strickler, *Nucl. Fusion* **26**, 769 (1986).
 - [4] J.E. Menard *et al.*, *Nucl. Fusion* **56**, 106023 (2016).
 - [5] F. Najmabadi and The ARIES Team, *Fus. Engineering and Design* **65**, 143 (2003).
 - [6] J.E. Menard, M.G. Bell, R.E. Bell, D.A. Gates, S.M. Kaye, B.P. LeBlanc, R. Maingi, S.A. Sabbagh, V. Soukhanovskii, and D. Stutman, *Phys. Plasmas* **11**, 639 (2004).
 - [7] R. Raman and V.F. Shevchenko, *Plasma Phys. Control. Fusion* **56**, 103001 (2014).
 - [8] G.D. Garstka *et al.*, *Nucl. Fusion* **46**, S603 (2006).
 - [9] E.A. Unterberg *et al.*, *J. Fusion Energy* **26**, 221 (2007).
 - [10] D.A. Gates and the NSTX National Research Team, *Phys. Plasmas* **10**, 1659 (2003).
 - [11] M. Gryaznevich *et al.*, *Phys. Rev. Lett.* **80**, 3972 (1998).
 - [12] E.J. Strait, T.S. Taylor, A.D. Turnbull, J.R. Ferron, L.L. Lao, B. Rice, O. Sauter, S.J. Thompson, and D. Wróblewski, *Phys. Rev. Lett.* **74** 2483 (1995).
 - [13] J.R. Ferron *et al.*, *Phys. Plasmas* **12**, 056126 (2005).

-
- [14] D.J. Battaglia, M.W. Bongard, R.J. Fonck, and A.J. Redd, Nucl. Fusion **51**, 073029 (2011).
- [15] D.J. Battaglia, M.W. Bongard, R.J. Fonck, A.J. Redd, and A.C. Sontag, Phys. Rev. Lett. **102**, 225003 (2009).
- [16] K.E. Thome, M.W. Bongard, J.L. Barr, M.G. Burke, R.J. Fonck, D.M. Kriete, J.M. Perry, and D.J. Schlossberg, Nucl. Fusion **57**, 022018 (2017).
- [17] M.G. Burke, J.L. Barr, M.W. Bongard, R.J. Fonck, E.T. Hinson, J.M. Perry, J.A. Reusch, and D.J. Schlossberg, Accepted, Nucl. Fusion (2017) doi: 10.1088/1741-4326.
- [18] D.J. Schlossberg, G.M. Bodner, M.W. Bongard, R.J. Fonck, J.A. Reusch, and C. Rodriguez Sanchez, Rev. Sci. Instrum. **87**, 11E403 (2016).
- [19] M.G. Burke, R.J. Fonck, M.W. Bongard, D.J. Schlossberg, and G.R. Winz, Rev. Sci. Instrum. **83**, 10D516 (2012).
- [20] A.C. Sontag, S.J. Diem, R.J. Fonck, G.D. Garstka, E.A. Unterberg, and T.A. Thorson, Nucl. Fusion **48**, 095006 (2008).
- [21] O. Sauter, C. Angioni, and Y.R. Lin-Liu, Phys. Plasmas **6**, 2834 (1999); O. Sauter, C. Angioni, and Y.R. Lin-Liu, Phys. Plasmas **9**, 5140 (2002).
- [22] T. Fujita and the JT-60 Team, Nucl. Fusion **43**, 1527 (2003).
- [23] D.A. Gates *et al.*, Phys. Plasmas **5**, 1775 (1998).
- [24] Y. Ono, T. Kimura, E. Kawamori, Y. Murata, S. Miyazaki, Y. Ueda, M. Inomoto, A.L. Balandin, and M. Katsurai, Nucl. Fusion **43** 789 (2003).
- [25] W. D'haeseleer *et al.*, *Flux Coordinates and Magnetic Field Structure* (Springer-Verlag, Berlin, 1991).
- [26] A.H. Glasser, Phys. Plasmas **23**, 072505 (2016).
- [27] S.C. Hsu, M. Artun, and S.C. Cowley, Phys. Plasmas **3**, 266 (1996).
- [28] A. Sykes and the START, NBI, MAST and Theory Teams, Nucl. Fusion **39**, 1271 (1999).
- [29] D. Palumbo, Nuovo Cimento B **53**, 507 (1968).
- [30] Ya.I. Kolesnichenko, V.V. Lutsenko, and V.S. Marchenko, Phys. Rev. Lett. **82**, 3260 (1999).
- [31] Ya.I. Kolesnichenko, R.B. White, Yu.V. Yakovenko, Phys. Plasmas **9**, 2639 (2002).
- [32] H.R. Wilson *et al.*, Nucl. Fusion **44**, 917 (2004).
- [33] D.R. Mikkelsen, R.B. White, R.J. Akers, S.M. Kaye, D.C. McCune, and J.E. Menard, Phys. Plasmas **4**, 3667 (1997).
- [34] S.K. Kim, D.H. Na, J.W. Lee, M.G. Yoo, H.-S. Kim, Y.S. Hwang, T.S. Hahm, and Yong-Su Na, Nucl. Fusion **56**, 106006 (2016).
- [35] E.A. Lazarus *et al.*, Phys. Fluids B **4**, 3644 (1992).
- [36] D.J. Schlossberg, G.M. Bodner, M.W. Bongard, M.G. Burke, R.J. Fonck, J.M. Perry, and J.A. Reusch, <https://dx.doi.org/10.18138/1340695>.

Captions:

FIG. 1: High- β_t discharge parameters. (a) I_p and I_{TF} ; (b) \bar{n}_e ; (c) core T_i (diamonds) and T_e (squares); and (d) MHD fluctuations (vertically offset for clarity). Fig. 1(c) and solid black waveforms from ramped- B_t scenario.

FIG. 2: Kinetically-constrained reconstruction of $\beta_t = 95\%$, $\beta_N = 6.7$ scenario. (a) Equilibrium flux surfaces and vessel geometry; (b) safety factor; (c) current profile; and (d) plasma parameters.

FIG. 3: Kinetic measurements from Thomson scattering and impurity spectroscopy at 24.5 ms in ramped- B_t scenario of Fig. 2. (a) Electron temperature profile and core ion temperature; (b) electron density profile; and (c) electron pressure profile.

FIG. 4: Troyon plot of Pegasus LHI discharges (markers) and other high- and low- A tokamaks (hatched, shaded regions). Circles (triangles) denote constant (decreasing) $B_t(t)$. Solid (open) markers denote kinetic (scaled magnetic) β_t equilibrium reconstructions.

FIG. 5: MHD analysis of disruptive ramped- B_t discharge. (a) Measured $n = 1$ dB_z/dt fluctuations near time of disruption; (b) DCON calculated poloidal harmonic content of marginally-unstable configuration at no-wall β limit.

FIG. 6: High- β_t $|B|$ well formation. (a) Equilibrium flux surfaces (dotted blue), $|B|$ isocontours (solid black), and $|B|$ well (shaded red); (b) profiles of $|B|$ and its components along the plasma midplane.

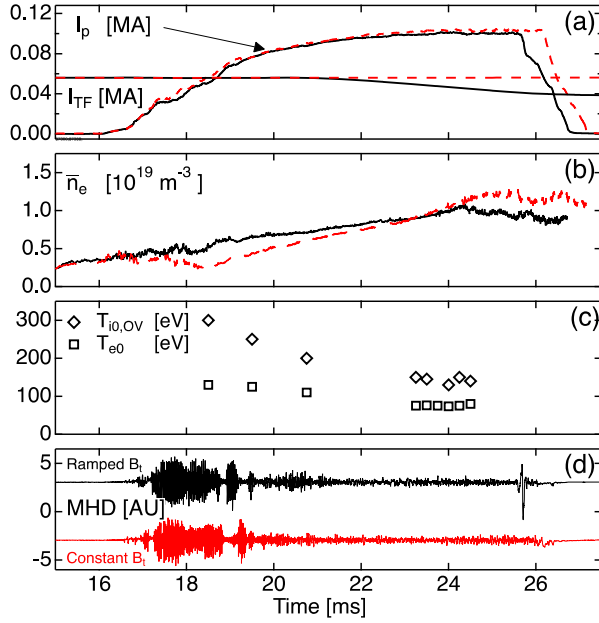


FIG. 1 High- β_t discharge parameters. (a) I_p and I_{TF} ; (b) \bar{n}_e ; (c) core T_i (diamonds) and T_e (squares); and (d) MHD fluctuations (vertically offset for clarity). Fig. 1(c) and solid black waveforms from ramped- B_t scenario.

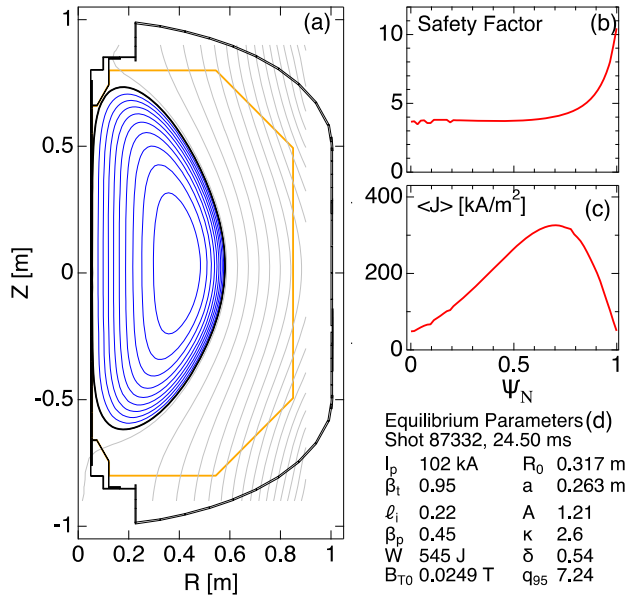


FIG. 2: Kinetically-constrained equilibrium reconstruction of $\beta_t = 95\%$, $\beta_N = 6.7$ scenario. (a) Equilibrium flux surfaces and vessel geometry; (b) safety factor; (c) current profile; and (d) plasma parameters.

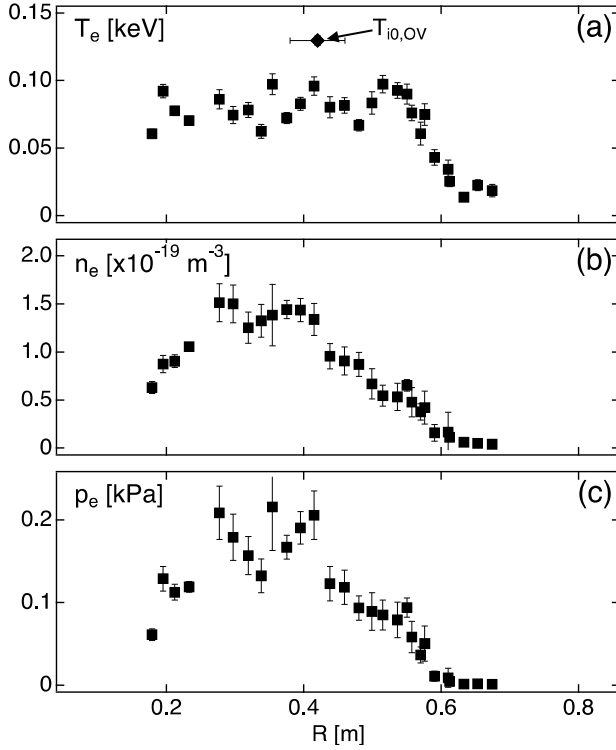


FIG. 3: Kinetic measurements from Thomson scattering and impurity spectroscopy at 24.5 ms in ramped- B_t scenario of Fig. 2. (a) Electron temperature profile and core ion temperature; (b) electron density profile; and (c) electron pressure profile.

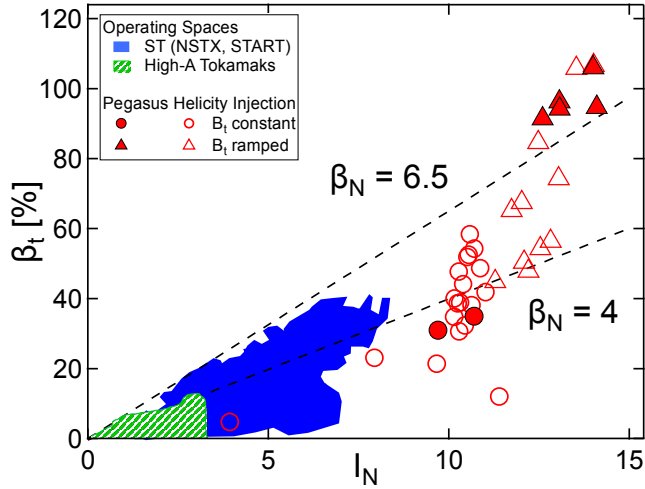


FIG. 4: Troyon plot of Pegasus LHI discharges (markers) and other high- and low- A tokamaks (hatched, shaded regions). Circles (triangles) denote constant (decreasing) $B_t(t)$. Solid (open) markers denote kinetic (scaled magnetic) β_t equilibrium reconstructions.

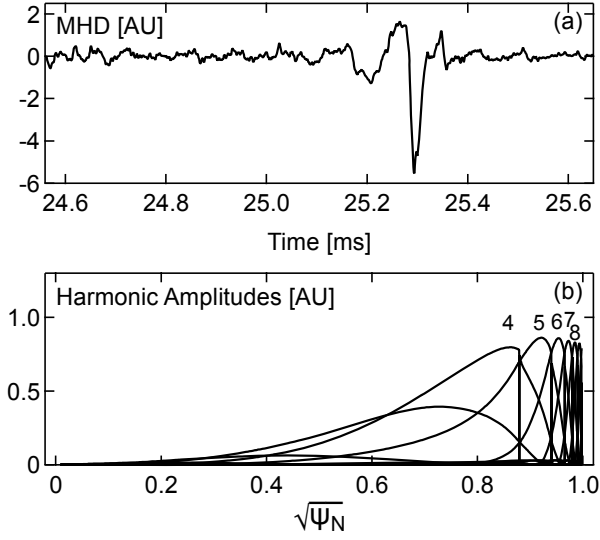


FIG. 5: MHD analysis of disruptive ramped- B_t discharge. (a) Measured $n = 1$ dB_z/dt fluctuations near time of disruption; (b) DCON calculated poloidal harmonic content of marginally-unstable configuration at no-wall β limit.

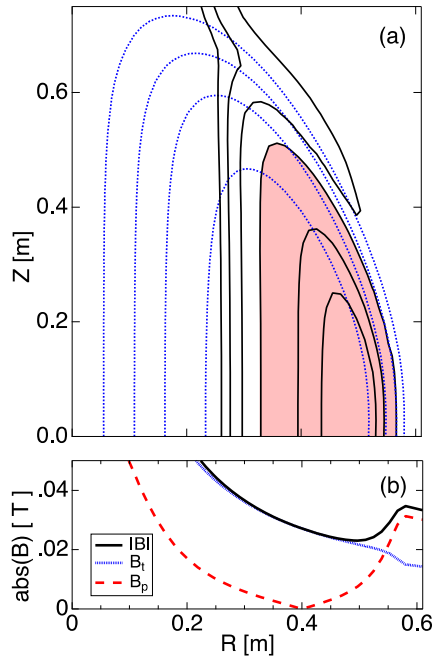


FIG. 6: High- β_t $|B|$ well formation. (a) Equilibrium flux surfaces (dotted blue), $|B|$ isocontours (solid black), and $|B|$ well (shaded red); (b) profiles of $|B|$ and its components along the plasma midplane.

